Combining single-station microtremor and gravity surveys for deep stratigraphic mapping

Giulia Sgattoni*, Dipartimento di Fisica e Astronomia, Alma Mater Studiorum - Università di Bologna, viale Carlo Berti Pichat 8, 40127 Bologna, Italy, email: giulia.sgattoni@unibo.it

Silvia Castellaro, Dipartimento di Fisica e Astronomia, Alma Mater Studiorum - Università di Bologna, viale Carlo Berti Pichat 8, 40127 Bologna, Italy, email: silvia.castellaro@unibo.it

*Corresponding author

Original paper date of submission: 9 October 2020

ABSTRACT

Any stratigraphic reconstruction by means of surface geophysical methods is affected by the non-uniqueness of data inversion and by the resolution-depth tradeoff. The combination of different geophysical techniques can reduce the number of degrees of freedom of the problem. We focus on two low-impact single-station geophysical techniques: microtremor and gravity. These have been used by previous authors for stratigraphic mapping only by comparing results independently. We suggest a procedure to combine microtremor and gravity data into a unique subsoil model and explore to what extent their combined use can overcome their individual weaknesses and constrain the final result. We apply the procedure to the Bolzano

sedimentary basin, Northern Italy, to derive a 3D bedrock model of the basin. We use microtremor data to map the ground resonance frequencies and derive an initial 3D bedrock depth model by assuming a Vs profile for the sediment fill. Then we define a density model for rock and sediments and perform a 3D gravity forward modeling. We then perturb both the Vs and density models and find the parameters best fitting the observed gravity anomalies. Data uncertainties are examined to explore the significance of the results. The joint use of the two techniques successfully helps interpreting the stratigraphic model: ground resonance frequencies guarantee spatial resolution of the bedrock geometry model while gravity data help constraining the frequency to depth conversion.

INTRODUCTION

Indirect geophysical methods are used for stratigraphic purposes in many geological contexts and at different survey scales. The intrinsic limitation of indirect methods is the need for constraints, due to non-uniqueness of geophysical data inversion. The issue can be overcome by constraining the model with independent direct stratigraphic information or by combining different geophysical techniques, each sensitive to specific model parameters. These cover a wide range of costs and amount of work needed. In this paper we focus on single-station geophysical techniques (microtremor and gravity), that are among the cheapest, lowest-impact and fastest geophysical approaches capable to map shallow and deep geologic structures (e.g., Komazawa et al., 2002; Brückl et al., 2007; McPhee et al., 2007). Other

traditional geophysical methods, such as seismic reflection, are more expensive and sometimes only limitedly or not applicable (e.g., in urban areas; Barnaba et al., 2010).

Microtremor and gravity single-station surveys have been combined for bedrock mapping in sedimentary basins (Komazawa et al., 2002; Barnaba et al., 2010; Özalaybey et al., 2011; Bottelin et al., 2019; Ferri et al., 2020). However, they were used only to qualitatively compare results independently. In this paper we aim to combine the two techniques and analyze them jointly in order to leverage their sensitivity to different physical parameters (i.e., Vs velocity and density) and minimize their individual limitations.

Single-station microtremor data are usually analyzed in terms of H/V ratio (horizontal to vertical spectral ratio; Nakamura, 1989). The H/V technique is a widespread tool to map resonance frequencies in seismic microzonation studies (Lermo et al., 1993, 1994; Lachet et al., 1996; Bour et al., 1998) and is used also for stratigraphic reconstructions by relating measured ground resonance frequencies with the thickness of the resonating layer, under some assumption on the shear wave velocity (Vs) subsoil profile. The first stratigraphic application of the H/V technique was proposed by Ibs von Seht and Wohlenberg (1999), who mapped the bedrock morphology in the Rhine valley. This was followed by other examples of subsurface mapping both shallow (tens of meters; e.g., Parolai et al., 2002; Castellaro and Mulargia 2009; Gosar and Lenart 2010; Mantovani et al., 2018) and deep (several hundred meters, up to >1 km; e.g., Zor et al., 2010; Sheib et al., 2016; Tarabusi and Caputo, 2016; Tün et al., 2016).

A limitation of the H/V method is represented by the availability of independent information to constrain the model in depth. Independent constraints can be either stratigraphic (on the depth of the resonating layers) or on the Vs velocities (e.g., Castellaro and Mulargia 2009). The uncertainty on the Vs profile estimates from surface-wave analyses is discussed in Foti et al. (2016). In addition, both types of information (Vs and depth of resonating layers) are often only available for the shallow subsurface, therefore the frequency-depth model is less resolved at depth.

Another limitation is represented by the role of 2D and 3D geometries (e.g., sedimentary basins) on measured resonances. The stratigraphic interpretation of H/V resonance peaks usually relies on a 1D assumption, i.e. on horizontally layered media. However, at sites with non-plane subsurface geometries, more complex resonance patterns may develop, such as 2D resonances that typically occur within sediment-filled valleys and involves simultaneous vibration of whole sediment fill. This phenomenon has been studied by several authors (e.g., Bard and Bouchon, 1980a,b; 1985; Chávez-García et al., 2000; Roten et al., 2006; Le Roux et al., 2012). Recently, Sgattoni and Castellaro (2020) described 1D versus 2D resonance patterns observed with single-station microtremor measurements and their impact on stratigraphic reconstructions. While 1D frequencies correlate with the local stratigraphy, 2D resonances are associated with the geometry of the whole resonating body, e.g., a sediment-filled valley. In this case, models to relate modal frequency ratios to the overall geometry of the valley cross-section can be applied (e.g., Bard and Bouchon, 1980a,b; Rial, 1989; Castellaro and Musinu, personal communication 2021).

The gravimetric technique is used for a wide range of survey scales. Several authors applied it to image the shape of buried valleys or sedimentary basins, where negative gravity anomalies are correlated with the buried morphology of the basement rock under the sedimentary fill. Some examples are, e.g., 2 km deep sedimentary basins in the Santa Rosa plain, San Francisco (McPhee et al., 2007), tens to hundred meters deep quaternary valleys in Lolland, Denmark (Møller et al., 2007), hundred meters deep glacial valleys in the Pyrenees (Perrouty et al., 2015) and 1.6-2.2 km deep grabens in western Turkey (Chakravarthi et al., 2017).

The success of the method depends on several factors, including the presence of an appreciable density contrast between sediments and bedrock, the possibility to identify the anomalies associated with the geological source of interest and the availability of independent constraints to effectively model the observed anomalies. As for all geophysical problems, the inherent ambiguity in gravity interpretation determines that the same gravity anomaly can be modeled with multiple different solutions (Skeels, 1947; Johnson and Van Klinken, 1979). This is an important limit for gravity measurements because they are sensitive to the 3D mass distribution around the measured site and a wide range of solutions match the same observed anomaly. The problem is enhanced by the presence of data errors, the estimation of which is not straightforward (e.g., Hinze et al., 2013).

In this paper we aim to optimize the joint use of microtremor and gravity data to derive a 3D bedrock model of the Bolzano sedimentary basin, Northern Italy. Microtremor data are used to create an initial 3D depth model of the basin from ground resonance frequencies by assuming a Vs pattern for the sediment fill. Then, we

define a density model for rock and sediments and perform a 3D gravity forward modeling. We then perturb both the Vs and density patterns and find the parameters better fitting the observed gravity anomalies. We account for data uncertainties to explore the significance of our results and to which extent combining the two types of data can help constraining the stratigraphic model.

METHOD OUTLINE

We propose a procedure to combine single-station microtremor and gravity measurements into a unique subsoil model. The method exploits ground resonances derived from microtremor measurements to build an initial subsurface model. This is then used for forward gravity modeling and optimized by perturbing the modeling parameters. We estimate model residuals normalized by data uncertainties for each set of parameters used in the calculation. This allows exploring the significance of the results and estimating the uncertainty due to the non-linearity of the problem. The workflow of the proposed methodology is shown in Figure 1 and consists in the following steps:

(1) identify ground resonance frequencies corresponding to the sediment-to-bedrock interface from single-station microtremor measurements (Figure 1a);

(2) estimate a shear wave velocity (V_S) profile for the sediment fill, either from other geophysical measurements, when available, or by fitting measured resonance frequencies to known bedrock depths (Figure 1b);

(3) build an initial bedrock-depth model by applying the relation between the fundamental ground resonance (f_0) and the thickness of the resonating layer (h, equation 1), by using the V_S model derived at the previous step (Figure 1c):

$$f_0 = \frac{V_S}{4h} \qquad (1)$$

(4) correct gravity measurements and derive residual gravity anomalies, together with an estimate of their uncertainties (Figure 1d);

(5) assign density values to the basement rock and sediment fill and perform 3D forward gravity modeling to compute the expected gravity along the investigated profiles (Figure 1e and 1f);

(6) repeat steps b), c) and e) for different Vs and density models; and

(7) evaluate the quality-of-fit of each run by using the reduced chi-square statistics and identify best fitting models (Figure 1f).

EXPERIMENTAL SETUP

The Bolzano alluvial sedimentary basin

The Bolzano basin (Northern Italy) lies at the junction between the Adige valley on the western and southern sides and two minor tributary valleys on the northern and eastern sides. It is a sedimentary basin filled with fine- to coarse-grained quaternary deposits of fluvio-glacial to lacustrine origin. The bedrock of the basin is made of Permian porphyritic rock (Figure 2).

Previous deep stratigraphic information within the basin is known only from reflection and H/V profiles (Figure 2; Pöyry 2017; Sgattoni and Castellaro 2020). According to these studies, the maximum depth of the basin ranges from about 400 m in the eastern portion to about 600-700 m where the basin intersects the Adige valley. Direct deep stratigraphic information is available about 20 km north west of the basin from a borehole located in the center of the Adige valley, which constrains the bedrock depth at 670 m (Bargossi et al., 2010).

SINGLE-STATION MICROTREMOR MEASUREMENTS

Identification of ground resonance frequencies

We acquired single-station microtremor recordings at 180 sites across the basin (Figure 2). The recordings were acquired during several field campaigns in winter, spring and summer of 2019 and 2020. Sgattoni and Castellaro (2020) already describe 60 of these measurements, distributed along three lines, and identify features to discern between 1D and 2D resonance patterns on both H/V functions and individual spectral components of motion. In the 1D case, a peak on the H/V curve is associated with a local minimum in the vertical spectral component (Figure 3), a feature related to lateral propagation of surface waves. 2D resonance, instead, is characterized by two distinct peaks in the horizontal spectral components, corresponding to the longitudinal and transversal (to the valley axis) resonance modes of the valley (Figure 3). In

addition, 2D frequencies do not vary in space while their amplitudes do, with maximum amplitudes observed close to the sites of maximum bedrock depth. We followed the same acquisition, processing and interpretation criteria as Sgattoni and Castellaro (2020) for the 120 new measurements to identify 1D and 2D-type resonances. As an example, one microtremor profile crossing the whole basin from west to east is reported as H/V contour plot in Figure 4. Here the red shades delineate the resonance peaks associated with the sediment-bedrock interface and 2D resonances are also marked. This profile spans a frequency range between about 0.28 Hz (which is the lowest observed resonance frequency within the basin) and 4.0 Hz (among the largest observed frequencies).

While 1D resonances depend on the local depth to bedrock and Vs by means of equation 1, 2D resonance frequencies depend on the whole valley aspect ratio. Numerical models can be used to infer the geometric properties of sediment-filled valleys from measured 2D resonances (Bard and Bouchon, 1980; Rial, 1989; Sgattoni and Castellaro, 2020; Castellaro and Musinu, personal communication, 2021), from which an estimate of the theoretical 1D resonance related to the deepest bedrock can also be obtained.

Based on the above-mentioned observations and models, we interpreted all single-station measurements to identify 1D resonance frequencies (measured or theoretical at sites where 2D resonance is observed) and infer the bedrock depth at each site, as discussed below.

Frequency to depth conversion

To convert resonance frequencies to depth by means of equation 1, a Vs model is needed. This is often inferred by assuming a power-law relation for the increasing Vs with depth (Ibs von Seht and Wohlenberg, 1999) and has been used by many authors in similar geologic settings (e.g., D'Amico et al., 2008; Özalaybey et al., 2011; Paolucci et al., 2015; Tün et al., 2016).

A Vs model can be derived by fitting resonance frequencies with known depths of the resonating layer, when independent stratigraphic information is available. We used the exponential model derived by Sgattoni and Castellaro (2020) using depth information down to 400 m from seismic reflection data (Figure 2b) and the corresponding resonance frequencies collected at 16 sites in the same area. These yield to the following frequency-depth relation:

$$H = 190 f^{-1.1} \quad (2)$$

where H is the bedrock depth and f is the ground resonance frequency.

Equation 2 is used to convert all the measured resonance frequencies to depths and interpolate them within a grid of points to obtain an initial 3D bedrock depth model.

GRAVITY MEASUREMENTS

Field acquisition

Four gravity survey lines were acquired within the Bolzano basin, consisting of a total of 49 measurement sites (red diamonds in Figure 2). The measurements were carried out in autumn 2019 and winter 2020 with a Lacoste & Romberg gravity meter model D. To remove the instrumental drift, we followed the looping technique by keeping each loop no longer than 2 hours so that the drift can be treated as a linear function of time. Each survey line was acquired in one day. Only profile EW1 was acquired in two days and in this case two points were repeated in both days to correct for the instrumental drift. The gravity measurements at the points overlapping between the profiles were also repeated. Almost all gravity stations are located in plane areas within the basin and care was taken in choosing measurement sites in flat areas and far from buildings.

Gravity surveys provide relative gravity measurements, which we did not convert to absolute gravity because this is not required for our scope. Each profile was then analyzed by calculating relative gravity anomalies to the beginning of each line.

Gravity data corrections

To derive the residual Bouguer gravity anomaly, we applied corrections for the instrumental drift, latitude, free-air, Bouguer slab, terrain, and regional gradient. The instrumental drift correction spans a range of ± 0.03 mGal, which is more than two orders of magnitude smaller that the observed gravity anomalies. The bedrock density used to compute the Bouguer slab and terrain corrections is 2600 kg/m^3, which is an

average value between the known rock densities measured around the basin (Material Testing Lab of the Autonomous Province of Bolzano, 2020, internal report).

To derive the measurement site elevations for the free-air and Bouguer corrections, we used a LiDAR-derived digital terrain model (DTM) with 0.5 m horizontal resolution and a declared relative elevation precision of 15 cm (Provincia Autonoma di Bolzano, 2013). Most gravity measurements were acquired on a flat or gently dipping topography within the basin, away from abrupt changes in elevation to avoid large uncertainties introduced by rugged topographies both on the elevation and in the terrain correction (LaFehr, 1991).

To compute the elevation and terrain corrections, and also for the forward modeling, the gravity values at each point of interest P were computed by summing the contribution of a number of segmented hollow cylinders of density ρ centered at the observation point P and with increasing radii, according to (Elkins, 1966; Figure 5a and 5b):

$$g_z = 2\pi G\rho \left[\sqrt{z_1^2 + r_2^2} - \sqrt{z_1^2 + r_1^2} - \sqrt{z_2^2 + r_2^2} + \sqrt{z_2^2 + r_1^2}\right], \quad (3)$$

where r_1 and r_2 are the inner and outer radii of the cylinder, z_1 and z_2 are the vertical distances of the top and bottom of the cylinder from P, and G is the gravitational constant. When using this equation for the terrain correction, z_1 lies either above or below the observation point depending on the topography. To account for the differences in elevation around the point of interest, each hollow cylinder was segmented according to the underlying DT model such that each cylinder segment approximates a DTM cell (Figure 5b) and the terrain correction is obtained by summing up the gravitational attraction of the columns around each measurement point (Figure

5c). The sum is calculated within a squared area around the point that can be extended within different distances from the observation site. We define the distance between the point and the perimeter of the square as the integration distance d_{int} (Figure 5c). This parameter can be varied in the calculation and DT models with varying resolution can be used depending on the distance from P.

For the calculation of the terrain correction we used DTMs with decreasing resolution with distance from each measurement site, i.e., 2.5 m x 2.5 m within 5 km (DTM from Provincia Autonoma di Bolzano, 2011), 50 m x 50 m between 5-40 km and 100 m x 100 m above 40 km (DTM from GMRT Map Tool; Ryan et al., 2009). A common approach is to calculate the topography mass contribution up to 167 km and even beyond (La Fehr, 1991). This is especially recommended in mountainous areas, when gravity measurements are distributed within a great range of station heights (Steinhauser et al., 1990). However, our survey is local and station elevations vary within 40 m (with the exception of three points only on the western edge of profile EW2 and on the northern edge of profile NS2). The limit of the region of interest is therefore expected to be lower than the standard value and we evaluated it by gradually increasing d_{int} until the relative change in terrain correction between the points becomes negligible. The correction in our case becomes almost stable at 5 km distance and changes slightly up to 50 km only along profile EW2. No difference is observed when increasing d_{int} up to 170 km (Figure 6). The thick yellow lines in the bottom row of Figure 6 are the corrected data, representing the Bouguer gravity anomalies along all four profiles. These curves clearly define the shape of negative

gravity anomalies with 6-7 mGal amplitude on average (note that values along the curves are relative for each profile).

Separation of the regional gradient

The Bouguer gravity anomaly can still be affected by regional changes due to large scale sub-surface mass variations such as isostatic mass adjustments and large-scale geological features at depth (Hinze, 1990; Hinze et al., 2013). However, as pointed out by LaFehr (1991), computing the separation between the regional and local gravity fields requires a broad knowledge of the regional geology, which is often not available.

A common approach is to model the regional component of the gravity field as a low-order polynomial, which operates as a low-pass filter separating the longer-wavelength regional component (e.g., Agocs, 1951; Coons et al., 1967; Beltrao et al., 1991; Thurston and Brown, 1992; Barnaba et al., 2010). The residual component is then estimated by subtracting the regional term from the observed anomaly. There is no general accepted rule on how this operation should be performed as this strongly depends on the wavelength of interest and on the amount and type of available data (e.g., auxiliary large-scale gravity data greatly improve interpretations, see Hinze et al., 2013).

By using regional gravity data available from ISPRA, ENI, OGS (2009) at the 1:250000 scale (Figure 7), we tested different strategies of surface fitting in order to estimate the regional gradient and its dependence on the chosen parameters. A

general east-west trend of the gravity gradient can be discerned from the map in Figure 7, which affects mainly the east-west profiles.

We fitted 2nd-, 3rd- and 4th-order polynomial surfaces within rectangular areas centered within the basin and extending up to distances of 1 km to 25 km from the investigated area. The residual anomalies obtained by subtracting these surfaces from the Bouguer anomalies of the two east-west trending profiles are shown in Figure 8. Because the fitted surfaces for the 3rd- and 4th-order polynomials showed no significant difference, we show them as a single plot in Figure 8b and 8d. In our case study, the choice of the polynomial degree has less influence compared to the size of the area used for the calculation, that causes substantial variation on the estimated regional trend. When increasing this area, the magnitude of the regional trend also increases but appears to stabilize at distances above 15 km. We do not have a way to define quantitatively the best estimate of the regional gradient, therefore we chose the parameters that seem to stabilize the trend and we estimated the uncertainty to account for the observed variations, as explained below. We used the regional trend estimated with a 3rd-order polynomial within a rectangular area extending up to 20 km distance from the investigated zone (Figure 7). We then subtracted this trend from each gravity profile to obtain the residual anomalies, which we consider as the component of the gravity field related to the sedimentary basin. The trend affects the east-west direction and is negligible along the north-south oriented gravity lines.

Uncertainties on gravity data

Estimating uncertainties associated with gravity data is not straightforward since the sources of error are many and difficult to be quantified. However, these can be relevant and we attempted to quantify them to infer the statistical significance of the obtained models.

While the instrumental reading accuracy can be considered quite small, on the order of 0.01 mGal (e.g., Ozaylaybey et al., 2011), the errors introduced by the data processing in the different steps of correction are larger and more difficult to evaluate.

Concerning the elevation correction (free air + Bouguer slab corrections), we estimated a range of uncertainties between 0.04-0.2 mGal depending on the location of the measurement points, either in flat areas or on the mountain sides. This accounts for elevation uncertainties of 0.2 to 1.0 m. While not negligible, this is still, conservatively, no more than one order of magnitude smaller than the amplitude of the observed gravity anomalies.

To estimate the uncertainty of the terrain correction, we repeated the calculation by adding random perturbations to the DTM grid to simulate ± 1 m elevation variations in the flat areas within the basin and ± 3 m elevation variations in the mountainous regions around the basin. Doing so generates errors (in terms of standard deviation) between ±0.03 mGal at sites located close to the center of the basin (far from rugged topographies) and ±0.1 mGal at sites located on the mountain sides.

To evaluate the uncertainty associated with the filtering of the regional trend we computed the deviation of the three different degrees polynomial surfaces for the

15-20-25 km distance areas at each measurement point. The resulting uncertainties for the two east-west profiles range from ±0.1 to ±0.5 mGal. Although this is a rough estimate, it shows that east-west profiles (EW1 in particular) are largely affected by errors in the estimation of the regional trend and this has to be accounted for when evaluating the goodness of the final model.

We then combined all the uncertainties at all measurement points by propagating errors through the additional operation of the gravity correction process. These range between 0.05 and 0.8 mGal. This is between one and two orders of magnitude smaller than the observed gravity anomalies. The largest uncertainties are observed along profile EW1 and at points measured on or close to the mountain sides.

Forward gravity modeling technique

We performed the gravity modeling with a forward, trial-and-error approach, which is widely used for the interpretation of gravity anomalies as it allows for full control on the modeling parameters (Hinze et al., 2013). We propose a simple method based on the same approach used for the terrain correction, using equation 3. Similar to the terrain correction, we built a conceptual model discretized into a grid with fixed horizontal coordinates (with 50 m x 50 m grid spacing). Each element of the model represents a vertical column with base level at the base of the sedimentary basin (Figure 5d). The mass contribution of each column to the gravity field at a given observation point on the surface is calculated in the same way as for the terrain correction, using the annular ring approximation (Figure 5). As for the terrain

correction, we tested different values of d_{int} until no change was observed in the shape of the modeled anomaly. More details will be discussed below.

With this approach, each column of the model can be assigned a different density, that can also vary vertically by subdividing the columns into segments. Columns falling outside the basin are assigned a unique constant rock density while columns within the basin are subdivided vertically into sub-columns with different densities: the bottom column segment is assigned the density of rock and overlying segments are assigned sediment density, either constant or with a vertical gradient (Figure 5d). The depth of the contact between rock and sediment density represents the sediment-bedrock interface at the base of the basin in geological terms. The mass contribution of each column segment is treated separately by means of equation 3 by varying z_1 and z_2 values depending on the vertical position of the column segment considered.

By starting from an initial model consisting of bedrock depth values assigned to each point of the grid (obtained from resonance frequencies) and a density model for the bedrock and sediment layers, we computed the expected gravity anomaly for the four profiles and compared the observed and modeled anomalies. We treated each profile independently and therefore analyzed results always relative to one end of each profile.

JOINT FIT RESULTS

Modeling parameters

We performed the gravity forward modeling with several Vs and density models. In addition to the Vs model in equation 2, we perturbed the coefficient and exponent of the power-law relation and built 15 Vs models (Figure 9) with different gradients of Vs with depth. We did this for two main reasons: first, to explore the capability of the gravity data to constrain the Vs model for the stratigraphic application of the H/V method, and second, to perform a sensitivity analysis of the gravity model to the bedrock geometries obtained with different Vs models.

We fixed a density of 2600 kg/m^3 for the porphyritic bedrock and tried several different models for the sediment fill. Direct information is available for the upper few meters to tens of meters only, for which known values are about 1800-1900 kg/m^3 (Material Testing Lab of the Autonomous Province of Bolzano, 2020, internal report). The basin fill is made of an alternation of fine- to coarse-grained deposits of fluvio-glacial to lacustrine origin but a detailed stratigraphic model is not available. We therefore chose to test several density models both with average uniform densities for the whole sediment fill (between 1900 and 2100 kg/m^3) and by assuming a vertical gradient of increasing density with depth. As noted by other authors (Cordell, 1973; Cai and Zhdanov 2015), the density-depth relationship of sedimentary rocks does not strictly follow specific mathematical formulations. We built six different density models (Table 1) which are similar to previous studies in the Adige valley (Rosselli et al., 2000) and plausible. Modeling gravity anomalies is sensitive to density contrasts, not to absolute density values; all density values should therefore be read as rock-to-sediment density contrasts. Also, the assumption of a constant rock density for the whole basin may not necessarily hold, as well as the lateral homogeneity of the

sediment fill. Our modeling scheme allows including lateral variations but we chose to keep the model as simple as possible (while still accounting for most of the observed gravity features, as shown in Section "Goodness-of-fit and final model"). Finally, we ran the gravity modeling by testing all the parameters discussed above, for a total of 90 models.

Goodness-of-fit and final model

To establish the best fitting model, we estimated the reduced chi-squared χ_r^2 for each model, i.e., the sum of the squared lengths of the deviations between observed and modeled gravity values normalized by their uncertainties, divided by the number of degrees of freedom. In general terms, $\chi_r^2 = 1$ means that the data are appropriately explained, $\chi_r^2 < 1$ means an overfit of the data and $\chi_r^2 > 1$ means the model does not explain the data to their level of uncertainty. This assumes that the model errors and data uncertainties are independent. This assumption does not necessarily hold in many cases, however it suffices to quantify the model-to-data fit compared to the data uncertainties. The problem is not linear and several different solutions fit the data equally well, so we want to both identify the set of solutions that explain the data within their uncertainty and estimate a threshold value for the data misfit below which models are to be discarded. This in turn helps us evaluate the uncertainty of the model due to its non-linearity.

We chose to include data uncertainties in the computation of the model deviation so that they act as weights, since data uncertainties differ considerably

between the different profiles and between points located on flat or rugged topography.

A note should be made concerning the evaluation of the model deviations. Because we deal with relative gravity measurements and we treat each profile separately in terms of differential gravity, the deviations between the modeled and measured anomalies depend also on the absolute shift of the reference measurement between model and observation. If this is not accounted for, then using different reference points leads to different measures of the model deviations. We accounted for this by shifting the modeled gravity anomaly by a value that minimizes the model deviations, which corresponds to the average of the differences between modeled and observed data. This is done separately for each profile and reduces the number of degrees of freedom by four units.

The resulting χ_r^2 values obtained for all Vs and density models are shown in Figure 10. The corresponding 12 models to 7 different Vs models (models n. 2, 4, 5, 6, 7, 8, 10), have $\chi_r^2 \leq 1$. This means that they fit well or overfit the data. In this case, overfitting the data simply means that the models fit observations to a degree that is below the estimated data uncertainties and therefore these models do not differ significantly between each other. We interpret these as a set of models each potentially representing an acceptable solution. All the remaining models are discarded.

The best gravity models are obtained for different combinations of the density and Vs values. This represents the inherent trade-off in the non-linear gravity model: the same fit can be achieved by increasing the sediment-bedrock density contrast

while decreasing the depth to bedrock. This is also the reason why model parameters, especially densities, were varied within pre-defined limits, to avoid testing for unreasonable model parameters. Adding more constraints from independent information helps further reducing the model variability.

We observe that among the seven best Vs models the one expressed by equation 3 is also included. As this Vs profile (red lines in Figure 9) was constrained with seismic reflection data, it was expected to result in a good data fit and represents our preferred solution. The corresponding modeled and measured gravity anomalies are shown in Figure 11 and the resulting 3D bedrock model is shown in Figure 12. The deviation observed between this model and the others gives an estimate of its uncertainty and gives also an idea of the expected depth deviation with different choices of the modeling parameters if no constraints were known. The estimated maximum depth of the basin is 700 m, which is consistent with stratigraphic information (Bargossi et al., 2010) and other geophysical analyses (Sgattoni and Castellaro, 2020). This value oscillates between 600-900 m when considering all the best solutions (i.e. the expected depth at the minimum observed resonance frequency, 0.3 Hz, for the seven best Vs models).

The modeled anomalies of Figure 11 are shown for different values of d_{int} from each calculated point. A stable result is obtained when this distance is equal to or larger than 700 m at profiles NS1, NS2 and EW2 and 1300 km at profile EW1. This tells us that the gravity field at each point is affected by the density distributions around the observation points up to distances between 700 m and 1300 m.

The largest deviations between measured and modeled gravity are observed on the western end of profile EW1. This may be due to an incorrect correction for the regional gradient (which largely affects this long profile oriented parallel to the maximum gradient) or to an incorrect depth modeling. The acquisition of more H/V and gravity data may help to better reconstruct the bedrock geometry in this part of the model.

The final 3D bedrock model suffers also from uncertainties on the experimental soil resonance estimations. These depend on the frequency and are higher for lower frequencies, as for any geophysical technique. As an example, a frequency deviation of 0.02-0.03 Hz at about 0.3 Hz, using Vs = 800 m/s, leads to a depth deviation of about 40-60 m, which is well within the depth range of the best models obtained with our modeling.

We note also that the best Vs models have in most cases a similar slope (expressed by the exponential coefficient of the power law), which suggests that the Vs model can be constrained by the combined use of microtremor and gravity data to some extent, i.e., the steepness of Vs increases with depth, and can be constrained in absolute terms if some independent information (e.g., on the density model or at least on one depth value) is available. Vice versa, if a velocity model is known a priori, some information can be gained on the density model that best fits the observations: in this case, if we use the velocity model 7, equally good fits are achieved with a uniform density model of the sediments with density equal to 2100 kg/m^3 (density model 6) and with increasing density with depth from 2000 to 2200 kg/m^3 (density model 2).

DISCUSSION

We performed a joint analysis of microtremor and gravity single-station measurements for stratigraphic reconstruction of a sedimentary basin. While previous studies (Komazawa et al., 2002; Barnaba et al., 2010; Özalaybey et al., 2011; Bottelin et al., 2019; Ferri et al., 2020) qualitatively combined the two techniques by comparing the two sets of data independently, here we propose an approach to combine them into a bedrock depth model with the aim of exploiting the strengths of the two geophysical techniques and overcoming their individual weaknesses. We applied the method to the Bolzano sedimentary basin (Northern Italy).

Microtremor measurements were used to infer ground resonance frequencies at 180 sites across the basin. We used the criteria described by Sgattoni and Castellaro (2020) to distinguish between 1D and 2D-type resonances and provide a stratigraphic interpretation.

The gravity data processing to derive residual anomalies was done by tuning the processing strategies for the specific problem and we aimed to track data uncertainties introduced by each step of the processing. The most problematic step was the estimation of the regional gradient, that affects our east-west oriented gravity lines. Common surface polynomial fitting strategies are dependent on several parameters, such as the size of the area used to perform the fitting. A convenient field practice to minimize the uncertainty related to the regional field separation may be to align measurements along profiles perpendicular to it. Estimated uncertainties on the

residual gravity anomalies range between 0.05-0.8 mGal, the largest being due to the regional gradient estimation and at points measured on or close to the mountain sides, due to uncertainties on elevation and terrain correction.

The combined analysis of ground resonance frequencies and gravity anomalies to derive a 3D bedrock model of the basin was done by (1) exploiting resonance frequencies to assess an initial bedrock model, by assuming an initial power-law Vs model for the sediment fill; (2) assuming an initial density model for sediments and rock and calculating a forward model of the residual gravity anomalies; (3) repeating the calculation for different Vs and density models, perturbed within reasonable bounds for the type of sediments filling the basin. With this process we were able to identify a set of solutions best fitting the observed gravity anomalies, corresponding to a set of best Vs and density models. This was done by selecting models with $\chi_r^2 \leq 1$, which indicate that the gravity data were fitted within and even below the estimated uncertainties. The deviation between these models gives an estimate of the uncertainty of the bedrock morphology, which is due to the non-linearity of the problem, i.e., the trade-off between different combinations of density and bedrock depth values, within the bounds of the modeling parameters tested. Among the best models, the one derived from regression analysis constrained with seismic reflection data is also included and we therefore choose this model as our preferred solution for our case study. We observe that seismic reflection profiles would benefit from a direct stratigraphic calibration, which is not available in this case.

The proposed 3D forward gravity modeling strategy is based on the same scheme commonly used for terrain corrections, it allows for flexibility on the model

geometry and density, has low computational cost, and the user has full control on the modeling parameters. Although it allows for complex density models, varying in both horizontal and vertical directions, we obtained a very good data fit with simple density models, even with uniform densities for both bedrock and sediment fill.

The combined use of microtremor and gravity data strengthens their stratigraphic applicability. Microtremor measurements are more sensitive to the local stratigraphy at the measurement site, while gravity measurements are affected by the 3D density distribution around the measured site and therefore have lower resolution in reconstructing the bedrock geometry. In addition, microtremor measurements are more sensitive to lithologic changes since Vs variability in the ground (100-3000 m/s) is larger than that expected for density (1600-2500 kg/m^3). The combined use of the two types of data therefore helps overcoming the strong non-linearity of the gravity modeling. Also, a difficult step in gravity modeling is building the initial model geometry, which is very important in a non-linear problem, and microtremor data can be used to build initial geometries. This in turn facilitates the use of a trial-and-error approach like the one suggested in this study.

When a Vs model is not known a priori, gravity measurements help constraining the model for the conversion of resonance frequencies to depths, given that a plausible range of densities for rock and sediments is available. We note that this depends also on the availability of gravity data for a wide range of bedrock depths. In our case study, more data on the shallower parts of the basin would likely help to better constrain the Vs model.

The combined use of microtremor and gravity data is effective also when few gravity profiles are available: the spatial resolution on the bedrock topography is guaranteed by the microtremor measurements while gravity data are used to constrain the frequency to depth conversion. In addition, gravity data can help in the interpretation of 2D effects on microtremor measurements. The shape of the gravity anomaly correlates with the bedrock geometry while 2D resonance frequencies do not vary across the resonating body. As an example, our EW2 profile shows an asymmetric gravity anomaly which supports an asymmetric bedrock shape.

CONCLUSIONS

The combination of microtremor and gravity techniques allow for extensive mapping of deep stratigraphic features. These are both low-cost single-station techniques that can be carried out by a single person and are therefore easily applicable to a broad range of scales and settings (including urban areas) as opposed to the more traditional seismic methods performed along long profiles that are expensive and not always feasible. Like all indirect geophysical methods, they both suffer from uncertainties due to non-uniqueness of data inversion and therefore need calibration information. Since borehole data may not be available at large depths, the possibility to effectively combine the two techniques to obtain a constrained bedrock model poses interesting perspectives.

We have explained a procedure to combine ground resonances and residual gravity anomalies into a unique subsoil model. This is done by exploiting the sensitivity of resonance frequencies to local stratigraphy, which guarantees spatial resolution of

the bedrock topography reconstruction, and by using gravity anomalies to constrain the frequency to depth conversion. In addition, the use of a fast, forward gravity modeling technique allows for extensive testing of the modeling parameters and allows estimating the final model uncertainty. We show that this procedure is able to overcome intrinsic limitations of both techniques and reduces the amount of stratigraphic constraints needed to derive a subsoil model. We applied the method to a sedimentary basin at the junction of three alpine valleys in Northern Italy. Thanks to the ease of use and wide applicability of these single-station techniques, we believe the approach presented in this study is of interest for application to different geological contexts and exploration scales (e.g. landslides, volcanic deposits, different scale valleys, paleovalleys and basins).

ACKNOWLEDGEMENTS

This study was funded under a cooperation agreement between the Department of Physics and Astromony (University of Bologna) and the Geological Survey of the Autonomous Province of Bolzano. We thank Giovanni Lattanzi and Stephen Slivicki for their support during some field surveys, and Volkmar Mair, Corrado Morelli and Maurizio Cucato for providing stratigraphic data. We are grateful to Letizia Anderlini, Enrico Baglione, Sara Bruni and Enrica Quartini for the fruitful discussions. We also thank the anonymous reviewers and editor for their helpful comments.

REFERENCES

Agocs, W. B., 1951, Least-squares residual anomaly determination: Geophysics, **16**, 686-696.

Bard, P.-Y., and M. Bouchon, 1980a, The seismic response of sediment-filled valleys, Part I, The case of incident SH waves: Bulletin of the Seismological Society of America, **70**, 1263-1286.

Bard, P.-Y., and M. Bouchon, 1980b, The seismic response of sediment-filled valleys, Part 2, The case of incident P and SV waves: Bulletin of the Seismological Society of America, **70**, no. 5, 1921-1941.

Bard, P.-Y., and M. Bouchon, 1985, The two-dimensional resonance of sediment-filled valleys: Bulletin of the Seismological Society of America, **75**, 519-541.

Bargossi, G. M., G. Bove, M. Cucato, A. Gregnanin, C. Morelli, A. Moretti, S. Poli, S. Zanchetta, and A. Zanchi, 2010, Geological Map of Italy at the scale 1:50.000 Sheet 013 "Merano", ISPRA – Servizio Geologico d'Italia – Provincia autonoma di Bolzano.

Barnaba, C., L. Marello, A. Vuan, F. Palmieri, M. Romanelli, E. Priolo, and C. Braitenberg, 2010, The buried shape of an alpine valley from gravity surveys seismic and ambient noise analysis: Geophysical Journal International, **180**, no. 2, 715-733; https://doi.org/10.1111/j.1365-246X.2009.04428.x

Belträo, J. F., J. B. C. Silva, J. C. Costa, 1991, Robust polynomial fitting method for regional gravity estimation: Geophysics, **56**, 80-89.

Bottelin, P., G. Dufréchou, L. Seoane, M. Llubes, and B. Monod, 2019, Geophysical methods for mapping Quaternary sediment thickness: Application to the Saint-Lary basin (French Pyrenees): Comptes Rendus Geoscience, **351**, no. 6, 407-419; https://doi.org/10.1016/j.crte.2019.07.001.

Bour, M., D. Fouissac, P. Dominique, and C. Martin, 1998, On the use of microtremor recordings in seismic microzonation: Soil Dynamics and Earthquake Engineering, **17**, 465–474.

Brückl, E., J. Brückl, W. Chwatal, and C. Ullrich, 2010, Deep alpine valleys: examples of geophysical explorations in Austria: Swiss Journal of Geosciences, **103,** 329–344; https://doi.org/10.1007/s00015-010-0045-x

Castellaro, S., and F. Mulargia, 2009, VS30 estimates using constrained H/V measurements: Bulletin of the Seismological Society of America, **99**, 761–773.

Chakravarthi, V., K. Mallesh, and B. Ramamma, 2017, Basement depth estimation from gravity anomalies: two 2.5D approaches coupled with the exponential density contrast model: Journal of Geophysical Engineering, **14**, 303-315; https://doi.org/10.1088/1742-2140/aa5832

Chávez-García, F. J., D. Raptakis, K. Makra, and K. Pitilakis, 2000, Site effects at Euroseistest-II, Results from 2D numerical modeling and comparison with observations: Soil Dynamics and Earthquake Engineering, **19**, no. 1, 23–39.

Coons, R. L., G. P. Woollard, and G. Hershey, 1967, Structural significance and analysis of mid-continent gravity high: American Association of Petroleum Geologists Bulletin, **51**, 2381-2399.

D'Amico, V., M. Picozzi, F. Baliva, and D. Albarello, 2008, Ambient noise measurements for preliminary site-effects characterization in the urban area of Florence, Italy: Bulletin of the Seismological Society of America, **98**, no. 3, 1373–1388.

Elkins, T. A., 1966, Vertical gradient of gravity on axis for hollow and solid cylinders: Geophysics, **31**, 816-820.

Ferri, F., M. Di Filippo, and M. Di Nezza, 2020, Gravity study of the Norcia intermountain basin (central Italy): Bollettino di Geofisica Teorica e Applicata, **61**, no. 3, 293-308.

Foti, S., F. Hollender, F. Garofalo et al., 2018, Guidelines for the good practice of surface wave analysis: a product of the InterPACIFIC project: Bulletin of Earthquake Engineering, **16**, 2367-2420; https://doi.org/10.1007/s10518-017-0206-7

Gosar, A., and A. Lenart, 2010, Mapping the thickness of sediments in the Ljubljana Moor basin (Slovenia) using microtremor: Bulletin of Earthquake Engineering, **8**, 501–518.

Hinze, W., R. Von Frese, and A. Saad, 2013, Gravity and Magnetic Exploration: Principles Practices and Applications, Cambridge University Press, Cambridge. https://doi.org/10.1017/CBO9780511843129.

Ibs-von Seht, M., and J. Wohlenberg, 1999, Microtremor measurements used to map thickness of soft sediments: Bulletin of the Seismological Society of America, **89**, 250–259.

ISPRA, ENI, and OGS, 2009, Cartografia Gravimetrica Digitale d'Italia alla scala 1:250.000, http://www.sinanet.isprambiente.it/it/sia-ispra/download-mais/cartografia-gravimetrica-digitale, accessed 26 May 2020.

Johnson, B.D., and G. van Klinken, 1979, Some equivalent bodies and ambiguity in magnetic and gravity interpretation: Bulletin of the Australian Society of Exploration Geophysics, **10**, 109–110.

Keim, L., Mair, V. and C. Morelli, 2013, Inquadramento geologico regionale. In Carta Geologica dell'Alto Adige, guida ai percorsi geologici, Foglio 026 Appiano. LAC Firenze. https://maps.civis.bz.it/

Komazawa, M., H. Morikawa, K. Nakamura, J. Akamatsu, K. Nishimura, S. Sawada, A. Erken, and A. Onalp, 2002, Bedrock structure in Adapazari Turkey - A possible cause of severe damage by the Kocaeli: Soil Dynamics and Earthquake Engineering, **22**, 829–836.

Lachet, C., D. Hatzfeld, P. Y. Bard, N. Theodulidis, C. Papaioannou, and A. Savvaidis, 1996, Site effects and microzonation in the city of Thessaloniki (Greece) comparison of different approaches: Bulletin of the Seismological Society of America, **86**, no. 6, 1692-170.

La Fehr, T. R., 1991, Standardization in gravity redaction: Geophysics, **56**, no. 8, 1170-1178.

Le Roux, O, C. Cornou, D. Jongmans, and S. Schwartz, 2012, 1-D and 2-D resonances in an Alpine valley identified from ambient noise measurements and 3-D modeling: Geophysical Journal International, **191**, no. 2, 579-590.

Lermo, J., and F. J. Chávez-García, 1993, Site effect evaluation using spectral ratios with only one station: Bulletin of the Seismological Society of America, **83**, 1574-1594.

Lermo, J., and F. J. Chávez-García, 1994, Are microtremors useful in site response evaluation?: Bulletin of the Seismological Society of America, **84**, 1350-1364.

Mantovani, A., S. Valkaniotis, D. Rapti, and R. Caputo, 2018, Mapping the Palaeo-Piniada Valley Central Greece Based on Systematic Microtremor Analyses: Pure and Applied Geophysics, **175**, 865-881; https://doi.org/10.1007/s00024-017-1731-7.

McPhee, D. K., V. E. Langenheim, S. Hartzell, R. J. McLaughlin, B. T. Aagaard, R. C. Jachens, and C. McCabe, 2007, Basin Structure beneath the Santa Rosa Plain Northern California: Implications for Damage Caused by the 1969 Santa Rosa and 1906 San Francisco Earthquakes: Bulletin of the Seismological Society of America, **97**, no. 5, 1449-1457; https://doi.org/10.1785/0120060269

Møller, M. J., H. Olsen, C. Ploug, G. Strykowski, and H. Hjorth, 2007, Gravity field separation and mapping of buried Quaternary valleys in Lolland Denmark using old geophysical data: Journal of Geodynamics, **43**, 330-337.

Nakamura, Y., 1989, A method for dynamic characteristics estimates of sub-surface using microtremor on the ground surface: Quarterly Report of Railway Technical Research Institute, **30**, 25-33.

Özalaybey, S., E. Zor, S. Ergintav, and M. C. Tapirdamaz, 2011, Investigation of 3-D basin structures in the İzmit Bay area (Turkey) by single-station microtremor and gravimetric methods: Geophysical Journal International, **186**, no. 2, 883-894; https://doi.org/10.1111/j.1365-246X.2011.05085.x

Paolucci, E., D. Albarello, S. D'Amico, E. Lunedei, L. Martelli, M. Mucciarelli, and D. Pileggi, 2015, A large scale ambient vibration survey in the area damaged by May–June

2012 seismic sequence in Emilia Romagna, Italy: Bulletin of Earthquake Engineering, **13,** 3187–3206; https://doi.org/10.1007/s10518-015-9767-5

Parolai, S., P. Bormann, and C. Milkereit, 2002, New relationship between Vs thickness of sediments and resonance frequency calculated by the H/V ratio of seismic noise for the Cologne area (Germany): Bulletin of the Seismological Society of America, **92**, 2521-2527.

Perrouty, S., B. Moussirou, J. Martinod, S. Bonvalot, S. Carretier, G. Gabalda, B. Monod, G. Hérail, V. Regard, and D. Remy, 2015, Geometry of two glacial valleys in the northern Pyrenees estimated using gravity data: Comptes Rendus Geoscience, **347**, no. 1, 13-23; https://doi.org/10.1016/j.crte.2015.01.002.

Pöyry, 2017, Deep seismic profile commissioned by the Autonomous Province of Bozen/Bolzano (in German), Technical report.

Provincia Autonoma di Bolzano, 2011, Digital Terrain Model (2.5 x 2.5 m), Cartografia provinciale e coordinamento geodati - Ripartizione 28. Geoportale Alto Adige, http://geokatalog.buergernetz.bz.it/geokatalog/. Accessed April 2021.

Provincia Autonoma di Bolzano, 2013, Digital Terrain Model Solar Tirol (0.5 x 0.5 m), Cartografia provinciale e coordinamento geodati - Ripartizione 28. Geoportale Alto Adige, http://geokatalog.buergernetz.bz.it/geokatalog/. Accessed September 2020.

Rial, J. A., 1989, Seismic wave resonance in 3-D sedimentary basins: Geophysical Journal International, **99,** 81-90.

Rosselli, A., R. Olivier, and L. Veronese, 1998, Gravimetry applied to the Hydrogeological Research in the Large Alpine Valleys in Trentino Region: Studi Trentini di Scienze Naturali – Acta Geologica, **75**, 53-64.

Roten, D., D. Fäh, C. Cornou, and D. Giardini, 2006, Two-dimensional resonances in Alpine valleys identified from ambient vibration wavefields: Geophysical Journal International, **165**, no. 3, 889-905.

Ryan, W. B. F., S. M. Carbotte, J. O. Coplan, S. O'Hara, A. Melkonian, R. Arko, R. A. Weissel, V. Ferrini, A. Goodwillie, F. Nitsche, J. Bonczkowski, and R. Zemsky, 2009, Global Multi-Resolution Topography synthesis, Geochemistry Geophysics Geosystems, 10, Q03014, doi: 10.1029/2008GC002332

Scheib, A., P. Morris, R. Murdie, and C. Delle Piane, 2016, A passive seismic approach to estimating the thickness of sedimentary cover on the Nullarbor Plain Western Australia: Australian Journal of Earth Sciences, **63**, no. 5, 583-598.

Skeels, D.C., 1947, Ambiguity in gravity interpretation: Geophysics, **12**, 43–56.

Sgattoni, G., and S. Castellaro, 2020, Detecting 1-D and 2-D ground resonances with a single-station approach: Geophysical Journal International, **223**, no. 1, 471-487; https://doi.org/10.1093/gji/ggaa325

Steinhauser, P., B. Meurers, and D. Ruess, 1990, Gravity Investigations in Mountainous Areas: Exploration Geophysics, **21**, 161-168

Tarabusi, G., and R. Caputo, 2016, The use of HVSR measurements for investigating buried tectonic structures: the Mirandola anticline, Northern Italy, as a case study:

International Journal of Earth Sciences, **106**, 341-353; https://doi.org/10.1007/s00531-016-1322-3

Thurston, J. B., and R. J. Brown, 1992, The filtering characteristics of least-squares polynomial approximation for regional/residual separation: Canadian Journal of Exploration Geophysics, **28**, 71-80.

Tün, M., Pekkan, E., Özel, O., and Y. Guney, 2016, An investigation into the bedrock depth in the Eskisehir Quaternary Basin (Turkey) using the microtremor method. Geophysical Journal International, **207**, no. 1, 589-607.

Zor, E., S. Özalaybey, A. Karaaslan, M. C. Tapırdamaz, S. Ç. Özalaybey, A. Tarancıoğlu, and B. Erkan, 2010, Shear wave velocity structure of the İzmit Bay area (Turkey) estimated from active–passive array surface wave and single-station microtremor methods: Geophysical Journal International, **182**, no. 3, 1603-1618; https://doi.org/10.1111/j.1365-246X.2010.04710.x

TABLES

Density models	**Depth (m)**	**Density (kg/m^3)**
1	0-100, 100-200, >200	1900, 2000, 2100
2	0-100, 100-500, >500	2000, 2100, 2200
3	0-50, 50-100, 100-200, 200-500 >500	1900, 2000, 2100, 2200, 2250
4	0-inf	1900
5	0-inf	2000
6	0-inf	2100

Table 1. Density models of the sedimentary basin fill used for gravity modeling.

FIGURES

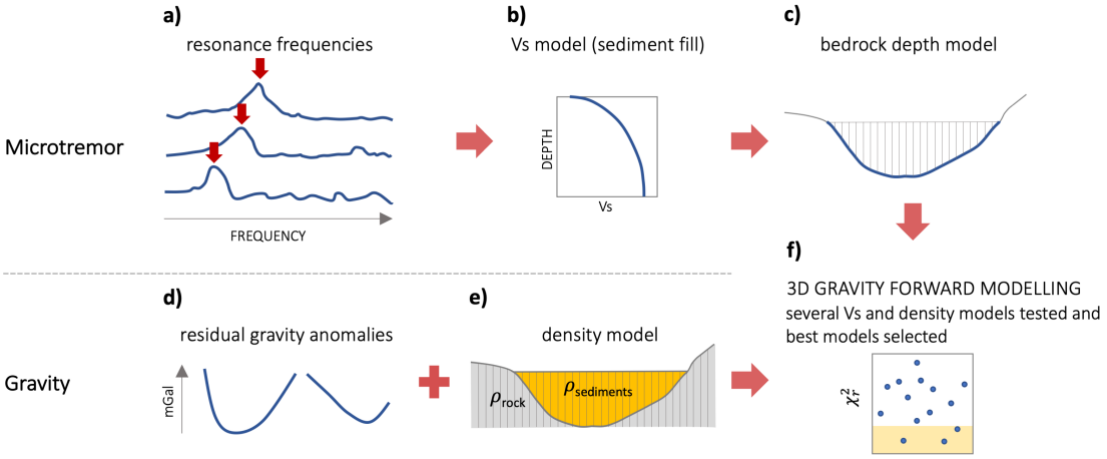

Figure 1. Flow-chart of the procedure proposed to combine single-station microtremor and gravity data into a 3D bedrock model. a) identification of ground resonance frequencies on single-station microtremor measurements; b) estimation of an average Vs profile for the sediment fill; c) frequency to depth conversion to build bedrock depth model; d) gravity data correction to derive residual gravity anomalies; e) estimation of rock and sediment densities; f) 3D gravity forward modelling for different combinations of Vs and density models. See text for further explanation.

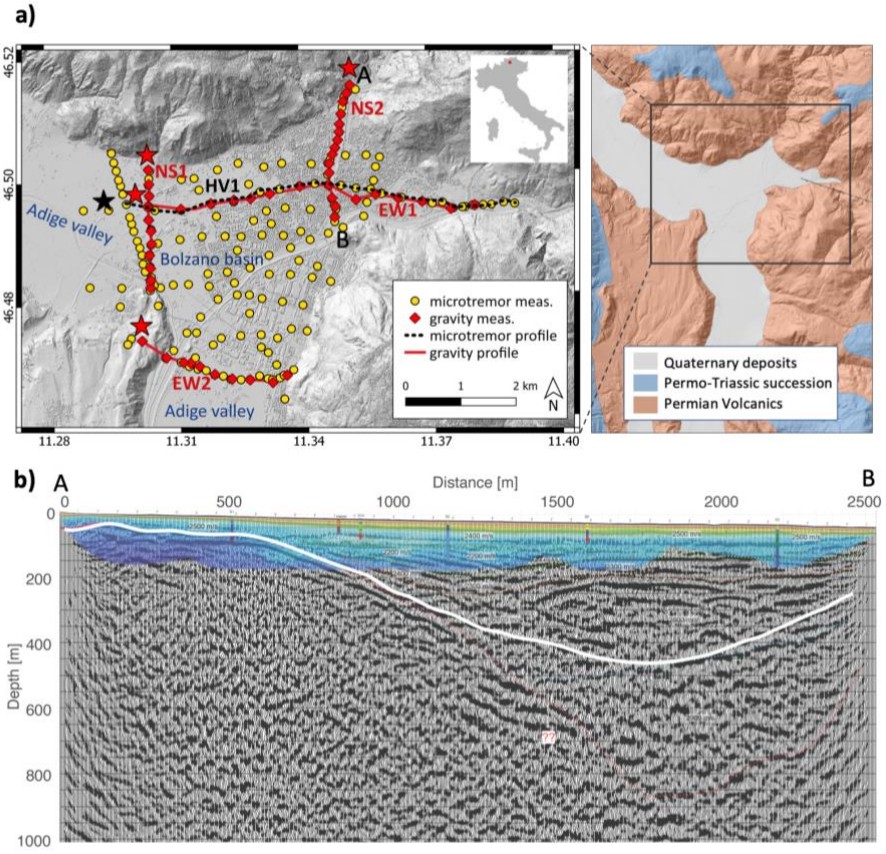

Figure 2. a) The Bolzano sedimentary basin (Digital Surface Model from Geoportale Alto Adige; geological map from Keim et al., 2013). NS1, NS2, EW1 and EW2 are the profiles along which gravity measurements were performed. HV1 is the profile of microtremor recordings shown in Figure 4. The stars indicate the starting point of the profiles and are drawn also in all the subsequent figures. b) reflection profile along line NS2 (Pöyry 2017). The white line indicates the sediment-bedrock interface.

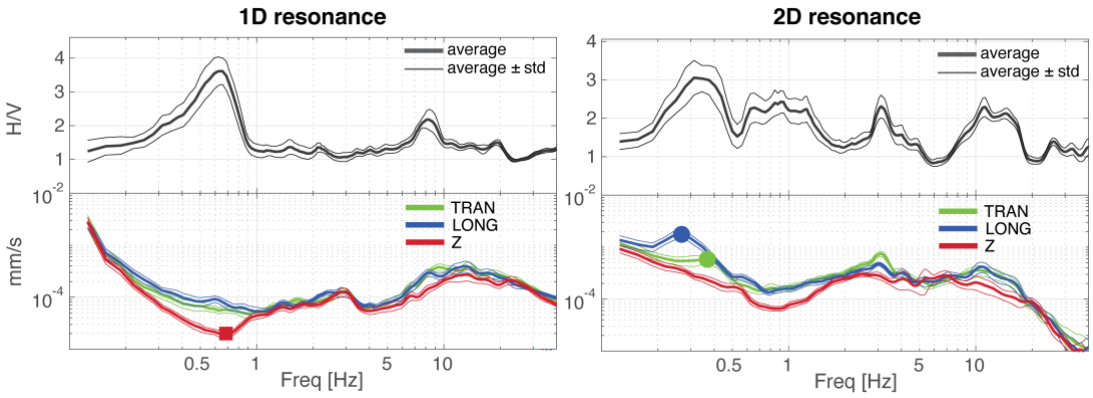

Figure 3. Examples of H/V curves and individual spectral components (longitudinal and transversal to the valley axis) for sites with 1D and 2D dynamic behaviors (modified from Sgattoni and Castellaro, 2020). For each H/V curve and individual spectrum, the confidence interval is given. The red square marks the minimum on the vertical spectral component at the 1D resonance frequency. The blue and green circles mark the longitudinal and transversal fundamental 2D resonance peaks.

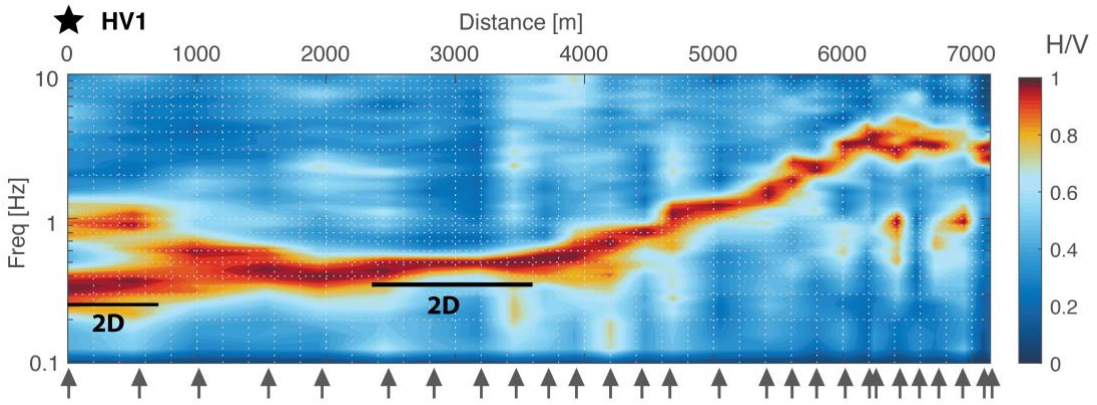

Figure 4. H/V contour plot of the HV1 profile. The star marks the starting point of the profile as indicated in Figure 1. Each H/V curve is normalized so that the color scale ranges from 0 (blue) to 1 (red). The arrows mark the positions of each measurement. The locations along the profile where 2D resonance is observed are indicated with black lines.

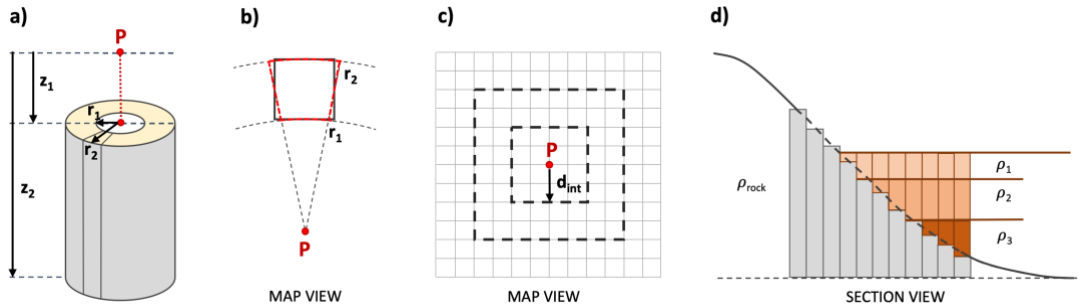

Figure 5. Gravity modeling approach, used for both terrain correction and modeling of the gravity anomalies. a) conceptual scheme for the application of Equation 3 for the gravity field of a hollow cylinder centered at the observation point (P). A segment of the annular ring is used as an approximation of each cell of the model (b), corresponding to one element of the grid in c) and one column in d). The

dashed squares in c) represent different areas within which the gravity effect is integrated and d_{int} is the integration distance. d) cross-section view of the conceptual model and density scheme used for the gravity forward modeling (discussed in Section "Forward gravity modeling technique"). The size of each cell depends on the DTM resolution used for the terrain correction or on the chosen discretization of the model. See text for further explanation.

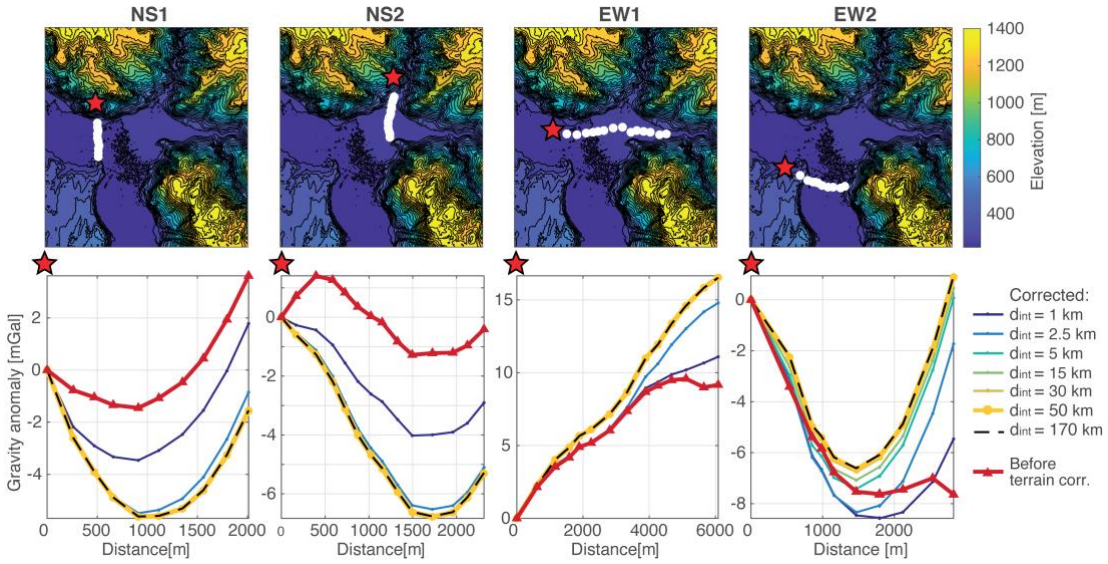

Figure 6. Terrain correction along the 4 investigated profiles. The top panels show the location of the profiles on a topographic map (corresponding to the red lines and stars in Figure 2) . The bottom panels show the original (in red) and corrected gravity data (in shades of blue, green, and yellow) after computing the terrain correction within different distances from each observation point (d_{int}). The final, accepted as corrected, data are represented by the thick yellow line.

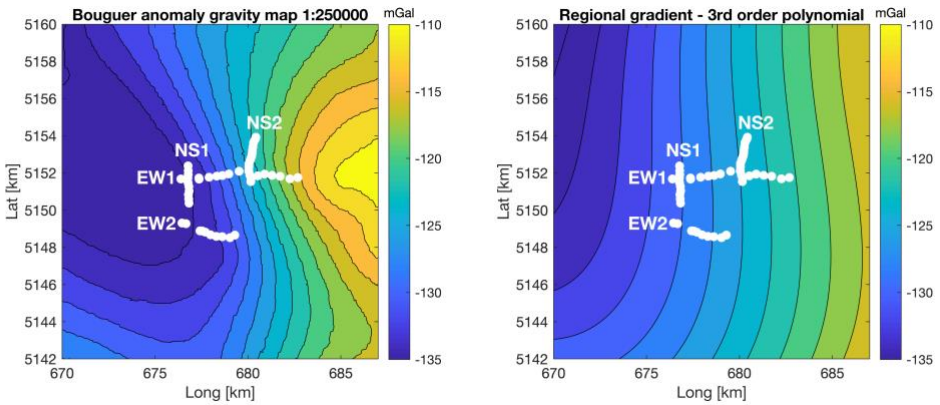

Figure 7. *Left:* Bouguer gravity anomaly from regional data a the 1:250000 scale from ISPRA, ENI, OGS (2009). *Right:* 3rd order polynomial surface fitting the data in a) computed with a rectangular area with perimeter 20 km distant from the investigated area. The white dots are the gravity measurements of this study.

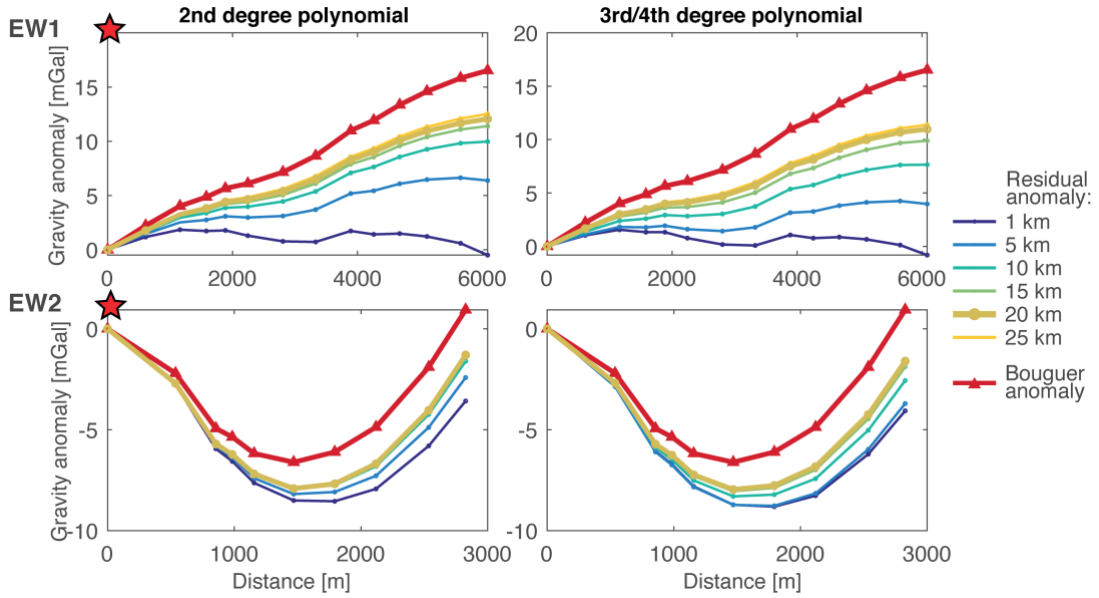

Figure 8. Separation of regional and residual gravity fields along profiles EW1 and EW2, with different order polynomials. The 3rd and 4th order polynomial surfaces are nearly coincident and are therefore shown in a single panel for each profile. The observed Bouguer anomalies are drawn in red. The blue, green, and yellow lines are the residual anomalies computed within increasing distances from the investigated area.

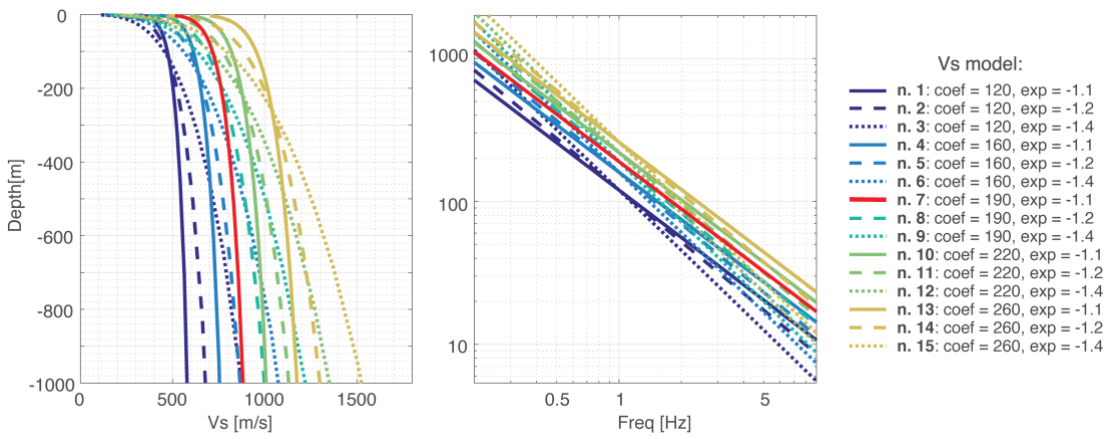

Figure 9. Power-law Vs models used to convert resonance frequencies to bedrock depths to build the bedrock depth model used for forward gravity modeling. The red line corresponds to the model in equation 2.

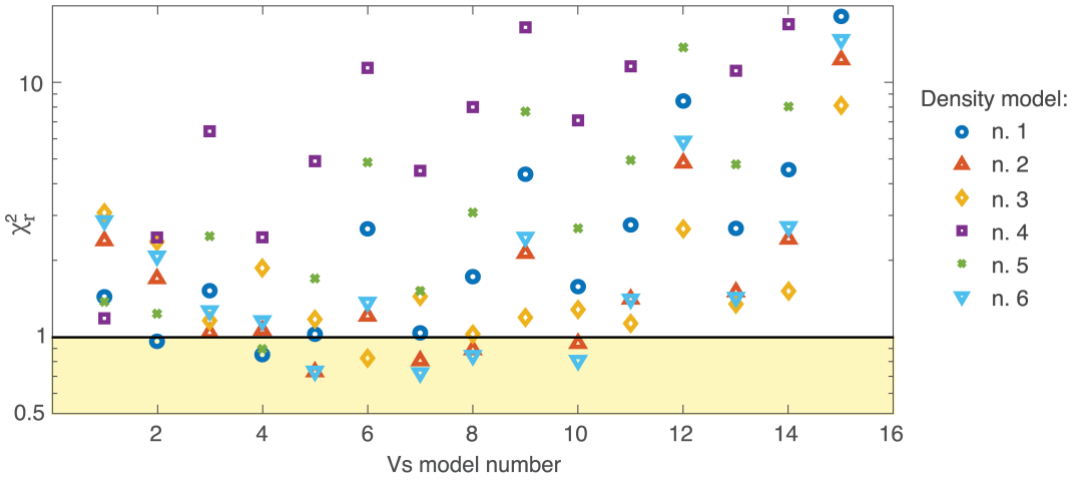

Figure 10. Reduced chi squared (χ_r^2) values obtained for all 90 models, as a function of Vs and density model number. The yellow area, below the horizontal line at $\chi_r^2 = 1$, highlights the set of best models which fit the data equally well with respect to the data uncertainty.

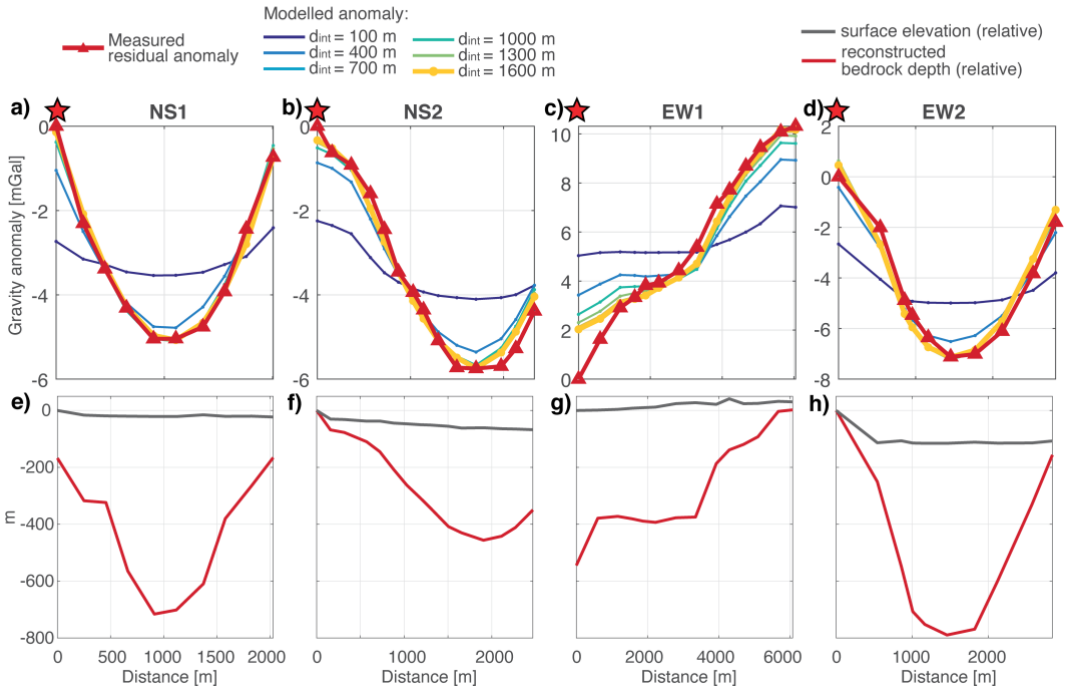

Figure 11. Final gravity model, obtained with density model n. 6 (Figure 10) and Vs model n. 7 (Figure 9, equation 2). Panels a), b), c) and d) show the surface and bedrock geometry along the 4 profiles (located as in Figure 2), relative to the left end of each profile. Panels f), g), h) and i) show the measured and modeled residual anomalies, the latter shown for increasing values of d_{int}.

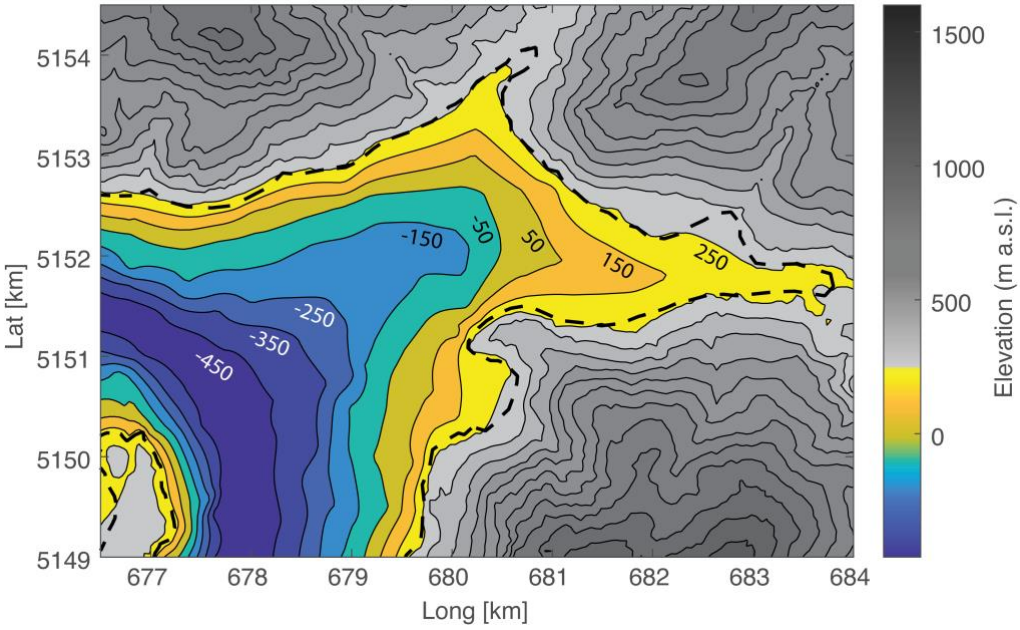

Figure 12. Final 3D bedrock model of the Bolzano basin obtained with the joint interpretation of resonance frequencies and gravity measurements. The black dashed line outlines the border of the sedimentary basin. Colored shades are used for the buried bedrock morphology and gray shades for the mountains around the basin. The darker blu color corresponds to bedrock depths of about 700 m. Contour lines interval: 100 m.